Kyvelou, P., Gardner, L. and Nethercot, D. A. (2017) Testing and Analysis of Composite Cold-Formed Steel and Wood-Based Flooring Systems. Journal of Structural Engineering. 143 (11), 04017146.

Testing and analysis of composite cold-formed steel and wood-based flooring systems

Pinelopi Kyvelou [a], Leroy Gardner [b], David A. Nethercot [c]

[a] Department of Civil Engineering, Imperial College London, SW7 2AZ, UK.
Email: pinelopi.kyvelou11@imperial.ac.uk. (Corresponding author)

[b] Department of Civil Engineering, Imperial College London, SW7 2AZ, UK.
Email: leroy.gardner@imperial.ac.uk

[c] Department of Civil Engineering, Imperial College London, SW7 2AZ, UK.
Email: d.nethercot@imperial.ac.uk

Abstract

An experimental study has been conducted into the degree of composite action that can arise between cold-formed steel joists and wood-based flooring panels. A series of material, push-out and four-point bending tests have been carried out, and alternative means of shear connection, featuring fasteners and adhesives, have been investigated. It has been found that the spacing of the fasteners as well as the application of structural adhesive at the beam-board interface has a significant influence on the attained degree of shear connection and hence the moment capacity and flexural stiffness of the system. The highest degree of shear connection (up to about 60%) was obtained using the structural adhesive, bringing corresponding increases in capacity and stiffness of around 100% and 40% respectively over the bare steel. Smaller, but still very significant, increases in capacity and stiffness were achieved through the use of screws alone. Based on the results of the push-out tests, a load-slip relationship for screw fasteners in wood-based floorboards has been proposed; this is designed for use in future analytical and numerical models. The findings of this research demonstrate, for the

first time, the benefits, in terms of enhanced structural performance and efficiency of material use, that can be derived through the practical exploitation of composite action in cold-formed steel flooring systems.

1 Introduction

Lightweight flooring systems comprising cold-formed steel joists and wood-based flooring panels are frequently employed for commercial, industrial and, more recently, residential buildings as they provide efficient, economical and durable solutions. However, unlike the case of hot-rolled steel beams and concrete slabs, where the benefits of composite action are well-known and effectively exploited, the interaction between cold-formed steel beams and the associated floor panels is generally ignored.

A number of investigations into composite action within cold-formed steel flooring systems have been carried out, usually involving the use of concrete slabs connected to the cold-formed steel beams. Abdel-Sayed (1982) and Wehbe et al. (2013) studied the structural behavior of systems comprising concrete beams and cold-formed channel sections, with the latter essentially serving as tension reinforcement. Hanaor (2000) and Lakkavalli and Liu (2006) carried out a series of large scale beam and push-out tests, investigating the performance of composite beams comprising cold-formed steel channel sections and concrete slabs connected with various fasteners to maximize the degree of shear connection. More recently, Alhajri et al. (2016) designed an innovative composite system of cold-formed steel beams and ferro-cement slabs, achieving substantial increases in load-carrying capacity over the bare steel system. A review of the research conducted into the development of composite action between concrete slabs and cold-formed steel beams has been presented by Bamaga et al. (2013).

Lawson et al. (2006) and Xu and Tangorra (2007) conducted experimental investigations into the serviceability performance of typical flooring systems comprising cold-formed steel C-shaped joists and wood-based boards, but did not consider the possible mobilization of composite action within such a system. It is only recently that Zhu et al. (2016) examined the structural behavior of systems with light-gauge steel truss girders and oriented strand boards and concluded that the distribution of the fasteners can have a significant influence on the stiffness and capacity of the system.

A preliminary experimental investigation performed by Kyvelou et al. (2015) on cold-formed steel beams of 1.5 mm thickness connected to wood-based floorboards showed that there is potential for significant improvement in the mechanical behavior of these systems if composite action can be mobilized; the key results of this investigation are summarized herein. These preliminary tests are supplemented by a series of additional experiments in the present paper – these include material tests to determine the basic stress-strain characteristics of the tested elements, beam tests carried out on similar flooring systems to those presented by Kyvelou et al. (2015) but employing cold-formed steel joists of 3 mm thickness and push-out tests to examine the load-slip characteristics at the steel-to-board interface considering both 1.5 mm and 3.0 mm thick steel. The key variable in the beam tests, and mirrored in the push-out tests, is the shear connection between the steel joists and the wood-based floorboards. The investigated means of shear connection were screws at various spacings and structural adhesive. The influence of the interface characteristics on the strain distribution, stiffness, strength and failure mode of the resulting composite systems is examined and discussed. The basis for a design method is presented and the key information necessary to implement the method is identified.

2 Material tests

Coupons taken from the cold-formed steel beams and floorboards of the main experiments were used for supplementary tests to determine the basic stress-strain behavior of the components of the flooring system.

2.1 Tensile steel coupon tests

For the determination of the material characteristics of the steel joists, four flat coupons and six corner coupons were extracted from the cold-formed steel sections, while an additional coupon was also cut from the coil prior to section-forming. The dimensions of the tensile coupons are given in Fig. 1, while the locations of the extracted coupons from within the steel sections are shown in Fig. 2. The coupon identification system begins with the letter C, followed by the nominal material thickness (e.g. 30 = 3.0 mm; 15 = 1.5 mm), followed by the coupon location with reference to Fig. 2, and finally, for repeated tests, the test number.

Two strain gauges were mounted on each coupon, one on either side, to accurately record longitudinal strains in the early stages of testing, while an optical extensometer was used over a 50 mm gauge length for larger strains. A detailed explanation of the tensile coupon testing procedure, which was conducted according to BS EN ISO 6892-1 (CEN 2009), is presented by Kyvelou et al. (2015). The measured material stress-strain curves, up to 2% strain, are illustrated in Fig. 3, while a summary of the key results is presented in Table 1. In Table 1, E is the Young's modulus, $\sigma_{0.2}$ is the yield (0.2% proof) strength, σ_u is the ultimate tensile strength, ε_u is the strain at the ultimate tensile stress, ε_f is the fracture strain measured over the standard gauge length (CEN 2009) and n and $n'_{0.2,1.0}$ are the strain hardening exponents of the two-stage Ramberg-Osgood material model proposed by Gardner and Ashraf (2006), which is a modification of that developed by others (Mirambell and Real 2000, Rasmussen 2003, Arrayago et al. 2015).

The key measured material properties of the 3 mm thick cold-formed steel are listed in Table 2, together with those of the previously tested 1.5 mm material (Kyvelou et al. 2015). It may be observed that the proof strength $\sigma_{0.2}$ of the corner coupons is, on average, 17% higher than that of the flat coupons. This is due to work hardening that arises from plastic deformations induced during section-forming (Karren 1967, Afshan et al. 2013, Rossi et al. 2013).

2.2 Material tests on wood-based floorboards

Coupons extracted from the floorboards were subjected to bending, compressive and tensile tests, which were performed according to BS EN 789 (CEN 2004b), in order to determine the material properties of the flooring panels. Three repeated tests were conducted for each test type and, for all tests, failure occurred within 4-6 min. Note that the same type of board was used for all tests, both for the 1.5 mm and 3.0 mm thick steel sections.

2.2.1 Bending tests

Four-point bending tests were carried out on specimens cut from the wood-based panels to determine the elastic modulus and strength of the material in bending. The dimensions of the specimens, which were defined in accordance with Clause 7.1 of BS EN 789 (CEN 2004b), as well as the experimental setup, are illustrated in Fig. 4. Three linear variable displacement transducers (LVDTs) were employed for the measurement of vertical deflections at midspan and at the loading points, as shown in Fig. 4(b). These three deflections were used to calculate curvature and hence the Young's modulus and strength in bending. The load was applied through a 750 kN Mayes Instron hydraulic actuator at a constant rate of 5 mm/min until failure. Load and displacement measurements were recorded using the Bluehill data acquisition system at 1 s intervals.

2.2.2 Compressive and tensile tests

Compressive and tensile coupons were tested to determine the elastic modulus and strength of the floorboard material in these two loading directions. The dimensions of the coupons were specified in accordance with BS EN 789 (CEN 2004b), and are presented in Fig. 5. Two strain gauges of 90 mm gauge length were attached to each coupon, one on either side. The load was applied through a 600 kN Instron loading frame at a constant axial rate of 0.5 mm/min for the compressive tests and 0.25 mm/min for the tensile tests. Strain and load measurements were recorded using the Bluehill data acquisition system at 1 s intervals.

2.3 Results

The key measured properties of the floorboard material, averaged from all repeated tests, are presented in Table 3. While the magnitudes of the elastic moduli in compression and tension were found to be similar, the elastic modulus in bending was significantly higher. The reason for this discrepancy, briefly presented by Kyvelou et al. (2015), relates to the stratified nature of the examined panels, which consisted of denser and hence stiffer material towards the external fibers and less dense material towards the mid-thickness of the board, as shown in Fig. 6. Since the strain is uniform over the cross-sectional area in the tensile and compressive tests, the influence of the denser material on the elastic modulus is not as beneficial as in the bending configuration, where the top and bottom fibers are subjected to higher strains and therefore make a larger contribution to the flexural stiffness.

In order for this explanation to be verified, the elastic modulus of the denser material of the floorboard was determined by means of an additional tensile test, where the less dense material situated towards the middle of the coupon had been extracted, as shown in Fig. 7. The elastic modulus of the denser material E_{dense} was found to be approximately 6.0 GPa, which is almost three times that determined from the tensile tests on the full board thickness.

A comparison of the initial parts of the stress-strain curves determined from the tensile coupon test described above and a typical tensile coupon test is presented in Fig. 8. The determined material properties are employed in the following section of this paper for the analysis of the beam test results, and will be used for incorporation into future finite element models.

3 Composite beam tests

3.1 Test specimens

A total of seven 4-point bending tests were conducted on flooring systems comprising cold-formed steel joists and wood-based particle boards with alternative means of shear connection, achieved with self-tapping screws at different spacings and structural adhesive at the beam-board interface. The cross-sectional shape of the tested steel beams as well as their average measured dimensions are presented in Fig. 9 and Table 4. The beam specimen identification system (e.g. B30-2) begins with the letter B, followed by the nominal material thickness (e.g. 30 = 3.0 mm) followed by the test number. A control test on a bare steel section (designated B30-1 for the 3 mm thick sections) was carried out to provide a reference response against which the remaining systems could be compared. For two specimens, wood adhesive was applied at the joints between adjacent floorboards to eliminate any gaps caused by the imperfect mating of the boards. A summary of the tested beam specimens is provided in Table 5, while typical cross-sections of the composite and bare steel beam tests are illustrated in Fig. 10. Note that the 1.5 mm thick beam specimens tested by Kyvelou et al. (2015) are also reported in Table 5.

Geometric imperfections of the beam specimens were measured prior to testing in order to obtain representative amplitudes for the local and distortional imperfection shapes (see Fig.

11), following the procedure adopted by Schafer and Peköz (1998). The determined imperfection magnitudes, which were expressed as a multiple of thickness (Schafer and Peköz 1998, Moreyra and Peköz 1994), were approximately 0.1*t* and 0.3*t* for the local and distortional mode shapes respectively.

3.2 Experimental setup

The overall experimental layout and the employed instrumentation for all beam tests are illustrated in Figs. 12 and 13 respectively. All beams, which were tested in pairs, were simply supported on rollers across a 5.8 m span with a 100 mm overhanging length from each support and were subjected to four-point bending. A spreader beam was used to transfer the load from the 250 kN Instron hydraulic jack, through loading plates, to two loading tubes running across the width of the floorboard. The surfaces between the loading tubes and the loading plates were lubricated to ensure that longitudinal movement was not inhibited and hence no net axial force would be introduced into the beam.

String potentiometers were employed for the measurement of vertical deflections at the midspan and loading points of each beam while longitudinal slip at the ends of the beams was recorded using four linear variable displacement transducers (LVDTs). End rotations were measured using inclinometers while the closing of the gaps between adjacent floorboards was measured using one extra LVDT positioned at the mid-width of the midspan section. Finally, strain gauges were mounted along the height and width of the midspan cross-section, as shown in Fig. 14, in order to monitor the strain distribution during testing. The strain gauge readings were used to determine the position of the neutral axes through the depth of the composite sections and to investigate shear lag effects across the board width.

At the supports and loading points, where the beams were subjected to high concentrated forces, the cross-sections were locally reinforced with a 150 mm length of steel beam of the

same section size, connected back-to-back with the specimen and wooden blocks, as shown in Fig. 15. This was to prevent localized failure of the beam web. At the same locations, wooden diaphragms were placed between the two parallel steel beams to prevent twisting and to help ensure their equal loading. For specimen B30-1, namely the bare steel test, 50×50×2 mm steel angles were used to inter-connect the top flanges of the two steel beams to provide lateral restraint, as shown in Fig. 16.

Each specimen was initially subjected to two loading cycles up to 10% of the expected ultimate capacity to ensure settling in of the specimen and correct functioning of the instrumentation; afterwards, load was gradually applied, up to failure, using displacement control at a rate of 2 mm/min. The electronic data acquisition system DATASCAN was employed for monitoring and recording the load, displacements, rotations, slip and strains, at 1 s intervals.

3.3 Test results

All specimens failed in-plane, with specimens B30-1 to B30-6 exhibiting distortional buckling of the top flange of the steel sections between the fixings (i.e. the screws) in the constant moment region, as shown in Fig. 17. The distortional buckling wavelength was found to decrease with reducing screw spacing – see Fig. 18. For the specimens employing wider screw spacing, the screws effectively restricted relative vertical displacement between the steel section and the board at their locations. However, for the specimens with denser screw spacing, distortional buckling was not fully restricted at the positions of the screws as these pulled through the floorboards. For specimen B30-6, distortional buckling was accompanied by screw failure. For specimen B30-7, tensile yielding of the bottom flange of the steel beam resulted in significant bending deformations and the test was stopped prior to the attainment of a clear peak at a vertical midspan displacement of 230 mm.

The load-displacement histories for all of the tested beams are shown in Fig. 19, where P_{exp} is the load applied to each beam and δ_{exp} is the vertical deflection at midspan. Reducing screw spacing, and the application of structural adhesive at the beam-board interface, resulted in higher degrees of shear connection and hence increasing strength and stiffness of the flooring systems. The recorded strain distributions through the depth of all specimens at ultimate load $P_{u,exp}$ and at 50% of $P_{u,exp}$ are illustrated in Fig. 20. It may be observed that as the degree of shear connection is enhanced, the position of the neutral axis in the steel migrates towards the top of the section – see Fig. 21. The neutral axis may also be seen to move further under increasing loading – this is attributed to closure of the gaps and greater engagement of the boards.

The readings from the strain gauges attached across the width of the boards at the midspan section are presented in Fig. 22. The results show that the boards were generally fully effective across their entire width and that shear lag effects were minimal. Thus, for the studied system, the effective width of the board b_{eff} can be taken as the beam spacing (i.e. b_{eff} = 600 mm).

The key experimental results obtained from all tests are listed in Table 6, where $M_{u,exp}$ is the moment capacity of each beam, $\delta_{u,exp}$ is the average vertical midspan deflection at ultimate load, $s_{u,exp}$ is the average slip at the ends of the beams at ultimate load, $(EI)_{exp}$ is the flexural stiffness of the flooring system and N_c is the compressive force in the floorboard at ultimate load, determined from the strain distributions of Fig. 20. The results for the previously tested 1.5 mm sections are also shown.

The ultimate moment capacity $M_{u,exp}$ and flexural stiffness $(EI)_{exp}$ of all specimens normalized by the moment capacity and flexural stiffness of the corresponding bare steel system are illustrated in the bar charts of Fig. 23. As expected, the systems comprising the

thinner steel sections benefitted to a greater extent from the mobilization of composite action due to the higher ratio of board area to steel area. For the 3 mm sections, increases in moment capacity of up to about 50% were achieved, while for the 1.5 mm sections, up to 100% increases were attained. In terms of flexural stiffness, increases of up to about 25% and 40% were achieved for the 3 mm and 1.5 mm sections, respectively. Comparisons between the pairs of specimens B30-2 and B30-3 and B15-3 and B15-4 also showed that there is benefit to be derived from the application of wood adhesive at the board joints.

3.4 Degree of shear connection

The attained degree of partial shear connection η is defined (CEN, 2004a) by the ratio:

$$\eta = \frac{N_c}{N_{c,f}} \tag{1}$$

where N_c is the compressive force in the board of the examined system and $N_{c,f}$ is the compressive force in the board of an equivalent system with full shear connection. The compressive force in the board at ultimate load of all tests N_c has been reported in Table 6 while $N_{c,f}$ can be determined from equilibrium considerations, as described in the following sub-section.

3.4.1 Theoretical fully composite system

The ultimate moment capacity of a fully composite system can be determined by assuming a plastic distribution of stresses, ignoring local buckling and considering the equilibrium of forces in the cross-section, as expressed by Equation (2) for the case in which the neutral axis lies within the steel section, where, with reference to Fig. 24, $N_{s,t}$ and $N_{s,c}$ are the plastic resistances of the portions of the steel section in tension and compression, respectively, and $N_{c,f}$ is the plastic resistance of the board in compression.

$$N_{s,t} = N_{s,c} + N_{c,f} \tag{2}$$

This may be expressed in terms of cross-sectional areas and material strengths by:

$$A_{st} f_y = A_{sc} f_y + A_b f_{cb} \tag{3}$$

where A_b is the cross-sectional area of the floorboard, f_{cb} is the compressive strength of the floorboard material, A_{st} and A_{sc} are the cross-sectional areas of the steel section in tension and compression respectively and f_y is the 0.2% proof strength $\sigma_{0.2}$ of the steel. The plastic neutral axis y_{pl} of the examined flooring system was found to lie within the steel for all the tested cross-sections.

The plastic moment capacity $M_{pl,R}$ of the composite section can be calculated by taking moments about the axis of the compressive force in the floorboard $N_{c,f}$:

$$M_{pl,R} = N_{s,t}(h_{tot} - t_b/2 - y_{s,t}) - N_{s,c}(h_{tot} - t_b/2 - y_{s,c}) \tag{4}$$

where h_{tot} is the total height of the composite cross-section, t_b is the thickness of the floorboard and $y_{s,t}$ and $y_{s,c}$ are the distances from the lower extreme fiber of the steel section to the centroids of the portions of the steel section in tension and in compression, respectively – see Fig. 24. Hence, assuming full shear connection for the examined system, the plastic compressive force in the board was found to be $N_{c,f}$ = 294 kN while the plastic moment capacity of the composite beam was calculated as $M_{pl,R}$ = 80.01 kNm for the 3 mm thick steel section and $M_{pl,R}$ = 44.79 kNm for the 1.5 mm thick steel section.

The second moment of area I_{comp} of the fully composite beam can be determined by transforming the area of the floorboard into an equivalent area of steel, as shown in Fig. 25, to account for the different stiffnesses of the components of the system. Hence, the area (or width) of the board is divided by the modular ratio:

$$n = E / E_{cb} \tag{5}$$

where E is the elastic modulus of the steel and E_{cb} is the elastic modulus of the board in compression. I_{comp} can then be calculated:

$$I_{comp} = I_{steel} + \frac{b_{eff} {t_b}^3}{12n} + A_s (y_{el} - y_c)^2 + \frac{A_b}{n} (y_{el} - h - t_b / 2)^2 \tag{6}$$

where I_{steel} and A_s are the second moment of area and area of the steel section respectively, y_{el} is the distance from the lower extreme fiber of the steel section to the centroid of the composite section and y_c is the distance from same point to the centroid of the steel section, as shown in Fig. 25. Hence, assuming full interaction, the second moment of area of the examined systems, determined according to Equation (6), is I_{comp} = 15.83 ×10^6 mm^4 for the 3 mm thick steel section and I_{comp} = 9.49 ×10^6 mm^4 for the 1.5 mm thick steel section. Note that the idealized centerline dimensions have been employed for the determination of the moment capacity and flexural stiffness of the fully composite system.

The experimental moment capacities $M_{u,exp}$ and flexural stiffnesses $(EI)_{exp}$ for all specimens normalized by the calculated moment capacity $M_{pl,R}$ and flexural stiffness $(EI)_{comp}$ of the equivalent systems assuming full shear connection are presented in Fig. 26. It may be observed that the more substantial the shear connection between the steel beam and the flooring board, the closer the moment capacities and flexural stiffnesses are to those of the equivalent fully composite system. As expected, the specimens employing the denser screw spacing and adhesive at the beam-board interface for both steel thicknesses (B15-5 and B30-7) performed best, with their moment capacity and stiffness reaching more than 80% of the capacity and stiffness of the equivalent fully composite systems. The systems comprising the thinner steel cross-section were generally able to develop a higher degree of composite action between the steel beams and the floorboards, as shown in Fig. 27, where the proportion of the

test capacity and stiffness between the bare steel and fully composite values are shown (with zero on the vertical axis being the capacity or stiffness of the bare steel section and unity being the capacity or stiffness of the theoretical fully composite section).

3.4.2 Attained degree of shear connection

The attained degree of shear connection η was calculated for all tested specimens according to Equation (1); the results are shown in Fig. 28. It should be mentioned that the values of η have been calculated with allowance for the nonlinear material behavior of the board while elastic behavior of the board was assumed by Kyvelou at al. (2015). Specimens B15-2 and B30-2, representing the typical current practice of securing the floorboards to the steel sections with screws at 600 mm centers, were found to achieve 4% and 10% of shear connection respectively, while over 60% shear connection was attained for the system employing the thinner steel beam and the structural adhesive at the beam-board interface (specimen B15-5). Overall, the results show that decreasing the spacing of the fasteners and the use of structural adhesive lead to higher degrees of partial shear connection and enable substantial mobilization of composite action within the systems. The load-slip responses of the employed shear connectors are examined through push-out tests in the following section.

4 Push-out tests

In order to determine the load-slip response of the shear connectors employed for the beam tests, push-out tests were performed. Schematic views of the test arrangement which featured two steel sections positioned back-to-back and boards connected to both sides in order to ensure a stable system during testing, are shown in Fig. 29. A summary of the tested specimens is listed in Table 7. The labelling system of the push-out specimens begins with the letter P, followed by the nominal steel material thickness and then followed by a number corresponding to the equivalent beam test employing the same shear connector arrangement.

For example, the specimen designated P30-5 corresponds to a push-out specimen comprising steel beams of 3.0 mm thickness and employing the same shear connector arrangement as beam specimen B30-5, namely self-drilling screws at 150 mm spacing.

The overall experimental setup is shown in Fig. 30. The load was applied through an Instron hydraulic actuator with a maximum load capacity of 750 kN. Four linear variable displacement transducers (LVDTs) were employed to measure the slip at the ends of both beams. All specimens were loaded until failure using displacement control at a displacement rate of 0.5 mm/min. The load and slip readings were recorded at 1 s intervals using the data acquisition system DATASCAN.

The measured load-slip (*P*-*s*) responses of all specimens are given in Fig. 31, where *P* is the load per connector (screw) and *s* is the average slip for the two steel sections. A summary of the obtained results is reported in Table 8, where P_u is the ultimate load per connector and s_u is the slip at ultimate load. It may be observed that all specimens exhibited very similar load-slip behavior except those that had structural adhesive at the beam-board interface (P15-5 and P30-7), where the response is considerably stiffer. For specimen P15-5, the load was carried by the adhesive bond up until the ultimate load while, for specimen P30-7, failure of the adhesive bond occurred prematurely, leading to lower ultimate capacity of the shear connection compared to that of specimen P15-5. Note that ultimate loads per connector P_u have not been reported for the P15-5 and P30-7 specimens since much of the load is carried through the structural adhesive.

Failure of all specimens ultimately occurred due to shear failure of the fasteners; however, significant bearing of the screws into the board was also observed, as shown in Fig. 32(a), and it is estimated that bearing deformations accounted for at least 80% of the total recorded slip at ultimate load s_u. Bending and shear failures of the fasteners are illustrated in Fig.

32(b). For the specimens with adhesive at the beam-board interface, the sharp drop in load after the initial stiff response corresponded to brittle failure of the adhesive bond.

Based on the recorded load-slip curves, a load-slip relationship for self-drilling screw fasteners connecting cold-formed steel beams and wood-based particle boards has been proposed, following the basic principles of the Ramberg-Osgood curve, comprising a linear and an exponential part. The general form of the relationship is given by Equation (7), with the coefficients C_1 and C_2 given by Equations (8) and (9).

$$s = \frac{P}{K_o} + C_1\left(\frac{P}{P_{10}}\right)^{C_2} \tag{7}$$

$$C_1 = s_{10} - \frac{P_{10}}{K_o} \tag{8}$$

$$C_2 = \frac{\ln\left(s_b - \frac{P_b}{K_o}\right) - \ln(C_1)}{\ln\left(\frac{P_b}{P_{10}}\right)} \tag{9}$$

where s_{10} is a slip of 10 mm, P_{10} is the load corresponding to s_{10}, K_o is the slip modulus of the employed connectors taken as the slope of the initial linear part of the push-out curve, P_b is the load corresponding to the bearing resistance of the floorboard in contact with the fastener, given by:

$$P_b = t_b d f_{cb} \tag{10}$$

and s_b is the slip on the push-out curve corresponding to P_b. Note that there may be situations where the load at a deformation of 10 mm is not reached, in which case an alternative deformation value may be employed. The shear resistance of the connector P_v constitutes the upper limit of the proposed curve and can be obtained from push-out tests as the ultimate load

per connector P_u, provided that ultimate failure is by shear, or taken as the ultimate load from individual shear tests on the connector or calculated based on the dimensions and material properties of the connector, as shown in Equation (11):

$$P_v = \pi \frac{d_{thr}^2}{4} \frac{f_u}{\sqrt{3}} \tag{11}$$

where d_{thr} is the threaded diameter of the employed connectors, usually equal to $0.75d$, and f_u is the ultimate tensile strength of the steel connector material.

A schematic representation of these key points is shown in Fig. 33(a), while the corresponding average measured values for the flooring systems studied in the current investigation are presented in Table 9. A comparison between the average experimental load-slip curve for specimens employing only self-drilling screws as shear connectors and the proposed model is shown in Fig. 33(b). The proposed model may be seen to capture accurately the load-slip response of self-drilling screws connecting cold-formed steel beams and wood-based floorboards, and is suitable for inclusion in future analytical and numerical models.

5 Conclusions

An experimental program including twelve beam tests, nine push-out tests and a series of material tests has been conducted in order to investigate the feasibility of developing composite action within cold-formed steel flooring systems and to quantify the derived benefits. It has been found that there is potential for significant improvements in the structural performance of cold-formed steel flooring systems by mobilizing interaction between the steel sections and the wood-based floorboards that they support.

The spacing of the fasteners, as well as the application of structural adhesive at the beam-board interface, were found to have a significant effect on the moment capacity and flexural stiffness of these systems, while the application of wood adhesive at the joints between adjacent floorboards led to further benefits. Increases in moment capacity of up to about 50% and 100% were achieved for the 3 mm and 1.5 mm thick steel sections, respectively. For flexural stiffness, the corresponding enhancements due to the mobilization of composite action were about 25% and 40% for the 3 mm and 1.5 mm thick steel sections, respectively. An outline of a design method that follows the principles of that commonly used for steel-concrete composite beams has been provided.

Based on the results of the conducted push-out tests, a load-slip relationship for self-drilling screw fasteners in wood-based floorboards has been proposed and is suitable for incorporation in future analytical and numerical models. Ongoing research involves the development of finite element models which, after validation against the obtained experimental data, will allow the influence of further key parameters to be examined and a full design method to be devised.

Acknowledgments

The authors would like to thank Ayrshire Metal Products for their funding of the experimental program as well as for their invaluable technical support, and Les Clark and Gordon Herbert for their work in the laboratory.

References

Abdel-Sayed, G. (1982). “Composite Cold-Formed Steel-Concrete Beams.” (1982). *ASCE J. Struct. Div.*, 108(ST11), 2609-2622.

Afshan, S., Rossi, B. and Gardner, L. (2013). “Strength enhancements in cold-formed structural sections – Part I: Material testing.” *J. Constr. Steel Res.*, 83, 177-188.

Alhajri, T.M., Tahir, M.M., Azimi, M., Mirza, J., Lawan, M.M., Alenezi, K.K. and Ragaee, M.B. (2016). “Behavior of pre-cast U-shaped Composite Beam integrating cold-formed steel with ferro-cement slab.” *Thin-Walled Struct.*, 102, 18-29.

Arrayago, I., Real, E. and Gardner, L. (2015). “Description of stress-strain curves for stainless steel alloys.” *Mater. Des.*, 87, 540-552.

Bamaga, S.O., Tahir, M.Md., Tan, T.C., Mohammad, S., Yahya, N., Saleh, A.L. Mustaffar, M., Osman, M.H. and Rahman, A.B.A. (2013). “Feasibility of developing composite action between concrete and cold-formed steel beam.” *J. Cent. South Univ.*, 20(12), 3689-3696.

CEN (European Committee for Standardization). (2004a). “Design of Composite Steel and Concrete Structures − Part 1-1: General Rules and Rules for Buildings.” *Eurocode 4, BS EN 1994-1-1*, Brussels, Belgium.

CEN (European Committee for Standardization). (2004b). “Timber structures – Test methods – Determination of mechanical properties of wood based panels.” *BS EN 789*, Brussels, Belgium.

CEN (European Committee for Standardization). (2009). “Metallic materials −Tensile testing− Part 1: Method of test at room temperature.” *BS EN ISO 6892-1*, Brussels, Belgium.

Gardner, L. and Ashraf, M. (2006). “Structural design for non-linear metallic materials.” *Eng. Struct.*, 28(06), 926-934.

Hanaor, A. (2000). “Tests of composite beams with cold-formed sections.” *J. Constr. Steel Res.*, 54, 245-264.

Karren, K.W. (1967). “Corner properties of cold-formed steel shapes.” *ASCE − Proc (J. Structural Div.)*, 93(ST1), 401-432.

Kyvelou, P., Gardner, L. and Nethercot, D.A. (2015). “Composite Action between Cold-Formed Steel Beams and Wood-Based Floorboards.” *Int. J. Struct. Stab. Dyn.*, 15(8), 1540029-1540046.

Lakkavalli, B.S. and Liu, Y. (2006). “Experimental study of composite cold-formed steel C-section floor joists.” *J. Constr. Steel Res.*, 62, 995-1006.

Lawson, R.M., Pedreschi, R., Ogden, R.G. and Grubb, P.J. (2006). “Developments in light steel composites in floors and roofs.” *Struct. Eng.*, 84(21), 44-50.

Mirambell, E., Real, E. (2000). “On the calculation of deflections on structural stainless steel beams: an experimental and numerical investigation.” *J. Constr. Steel Res.*, 54(1), 109-133.

Moreyra, M.E. and Peköz, T. (1994). “Finite element studies on lipped channel flexural members.” Proc., *12th Internat. Spec. Conf. Cold-Formed Steel Struct.*, St. Louis, Missouri, 57-74.

Rasmussen, K.J.R. (2003). “Full-range stress-strain curves for stainless steel alloys.” *J. Constr. Steel Res.*, 59(1), 47-61.

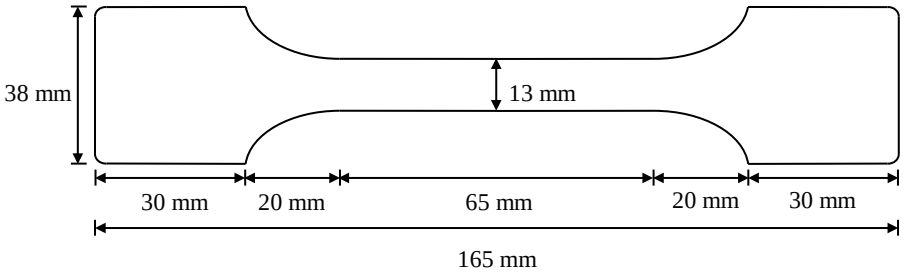
Rossi, B., Afshan, S. and Gardner, L. (2013). “Strength enhancements in cold-formed structural sections - Part II: Predictive models.” *J. Constr. Steel Res.*, 83, 189-196.

Schafer, B.W. and Peköz, T. (1998). “Computational modeling of cold-formed steel: characterizing geometric imperfection and residual stresses.” *J. Constr. Steel Res.*, 47(3), 193-210.

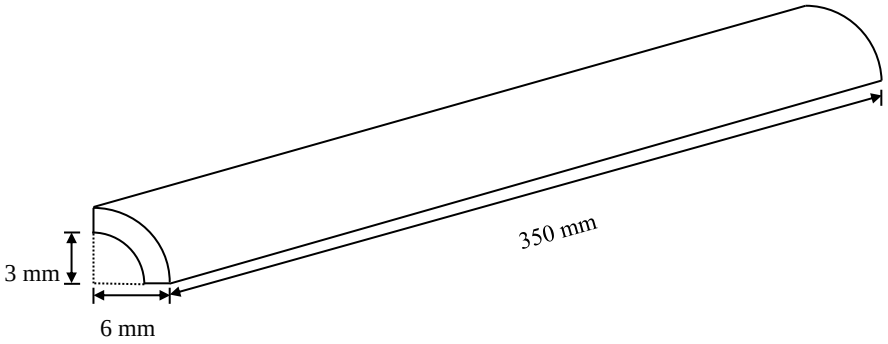
Wehbe, N., Bahmani, P. and Wehbe, A. (2013) “Behavior of Concrete/Cold Formed Steel Composite Beams: Experimental Development of a Novel Structural System”. *Ind. J. Concr. Struct. Mater.*, 7(1), 51-59.

Xu, L. and Tangorra, F.M. (2007). “Experimental investigation of lightweight residential floors supported by cold-formed steel C-shape joists.” *J. Constr. Steel Res.*, 63, 422-435.

Zhu, L., Yang, Y., Wang, Z. and Song, M. (2016). “Stability Analyses of the Upper Chord Tubes of Light Gauge Steel-Oriented Strand Board Composite Truss Girders.” *Int. J. Struct. Stab. Dyn.*, 16(1), 1640012 1-12.



(a)



(b)

Fig. 1. Dimensions of (a) flat and (b) corner tensile coupons

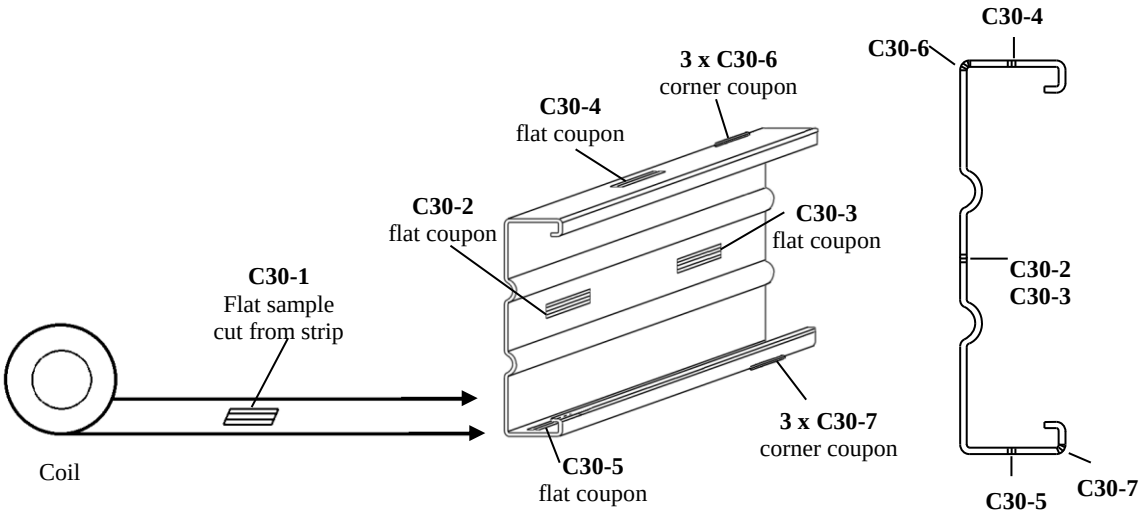


Fig. 2. Positions of extracted tensile coupons

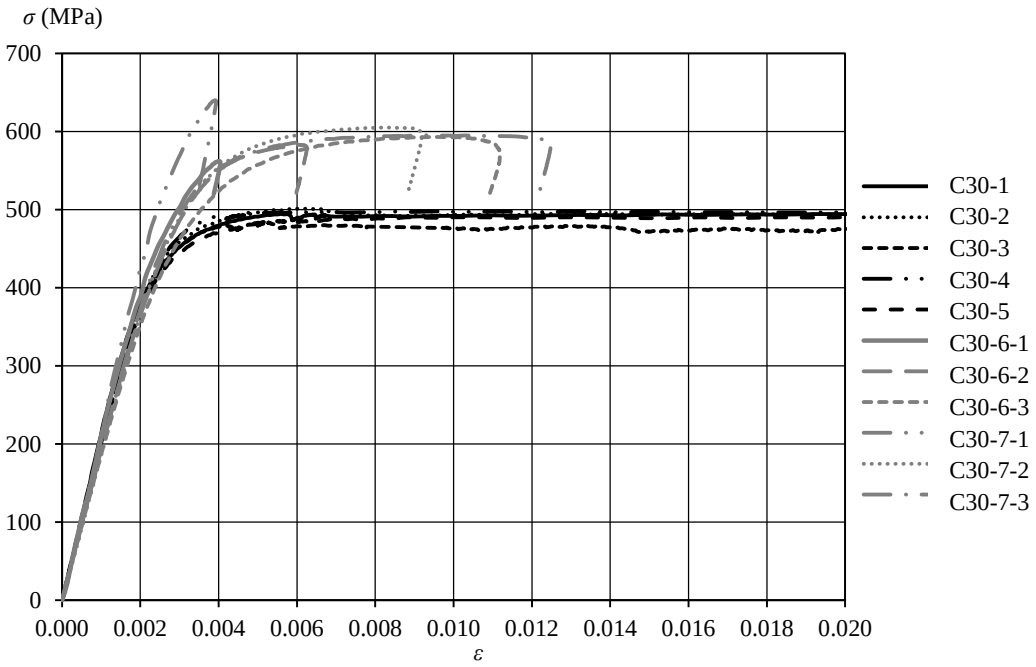
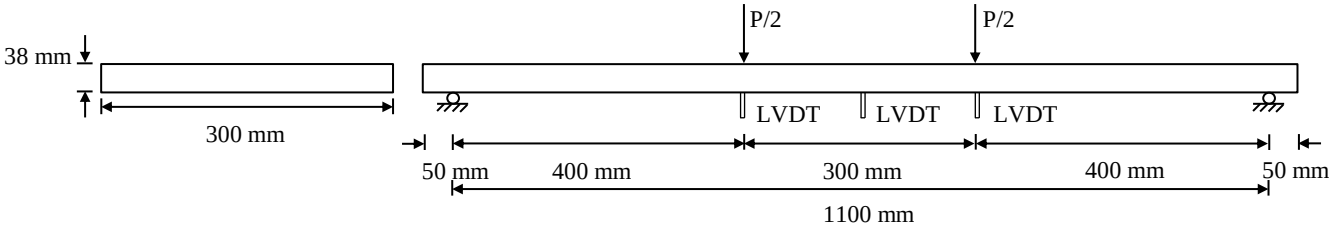


Fig. 3. Stress-strain curves obtained from tensile coupon tests



(a) Cross-section (b) Elevation

Fig. 4. Dimensions of (a) cross-section and (b) elevation of bending coupon tests

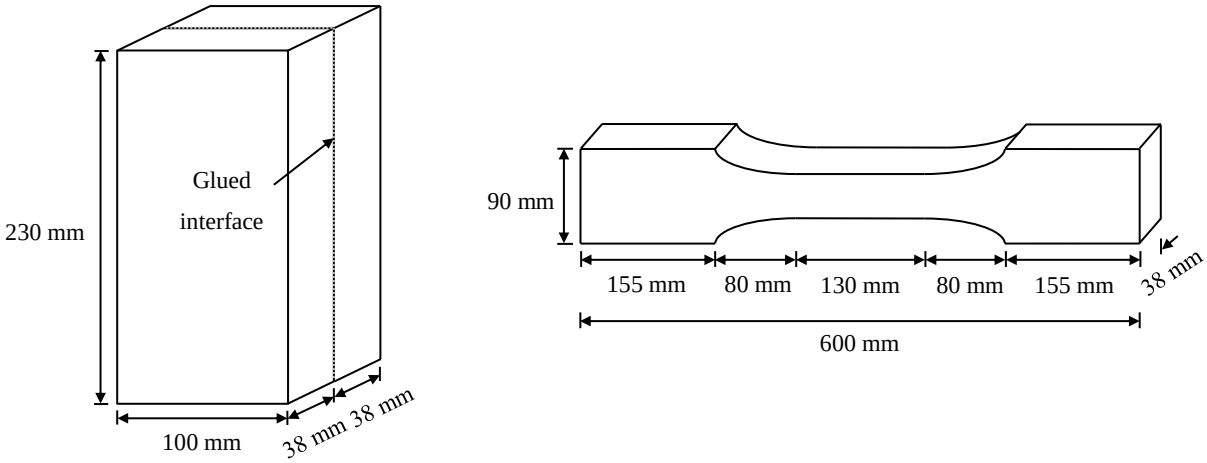


Fig. 5. Dimensions of (a) compressive and (b) tensile coupons

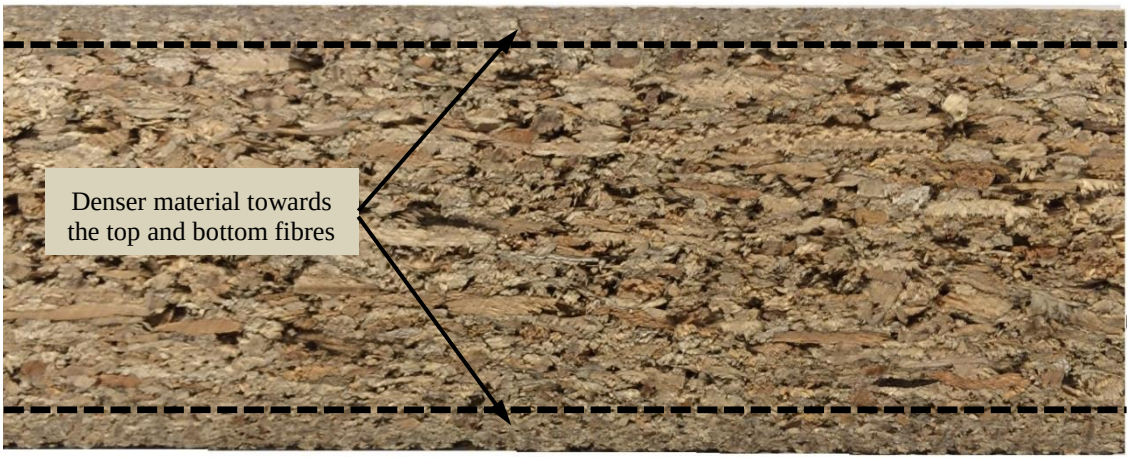


Fig. 6. Stratified flooring panel



Fig. 7. Tensile coupon tested for the determination of the elastic modulus of the denser material of the floorboards

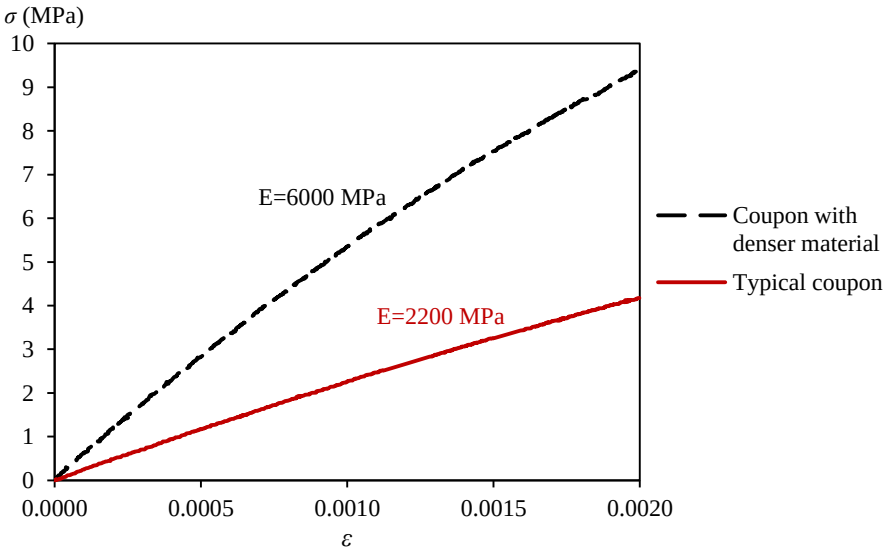


Fig. 8. Initial part of stress-strain curves of a typical (full board thickness) tensile coupon and of a tensile coupon with the less dense material removed

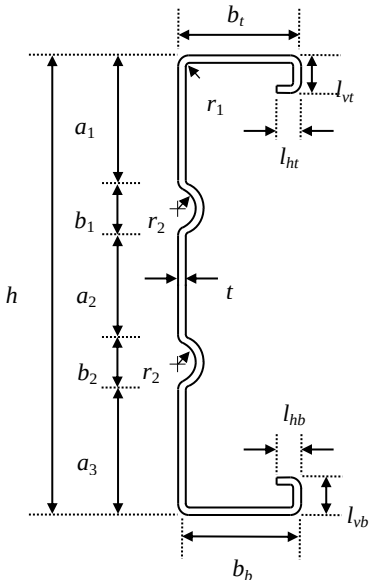


Fig. 9. Cross-sectional shape and labelling of dimensions of tested cold-formed steel joists

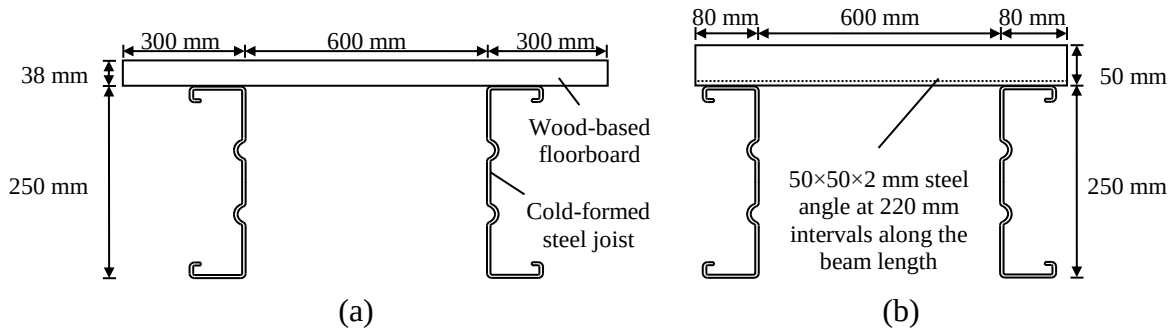


Fig. 10. Typical cross-section of (a) composite and (b) bare steel specimens

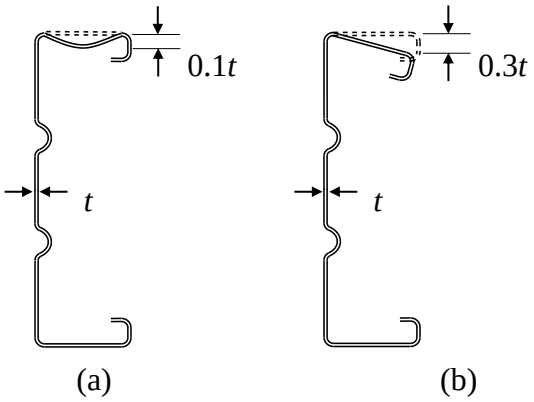


Fig. 11. Illustrative shapes of (a) local and (b) distortional imperfections of the steel beams

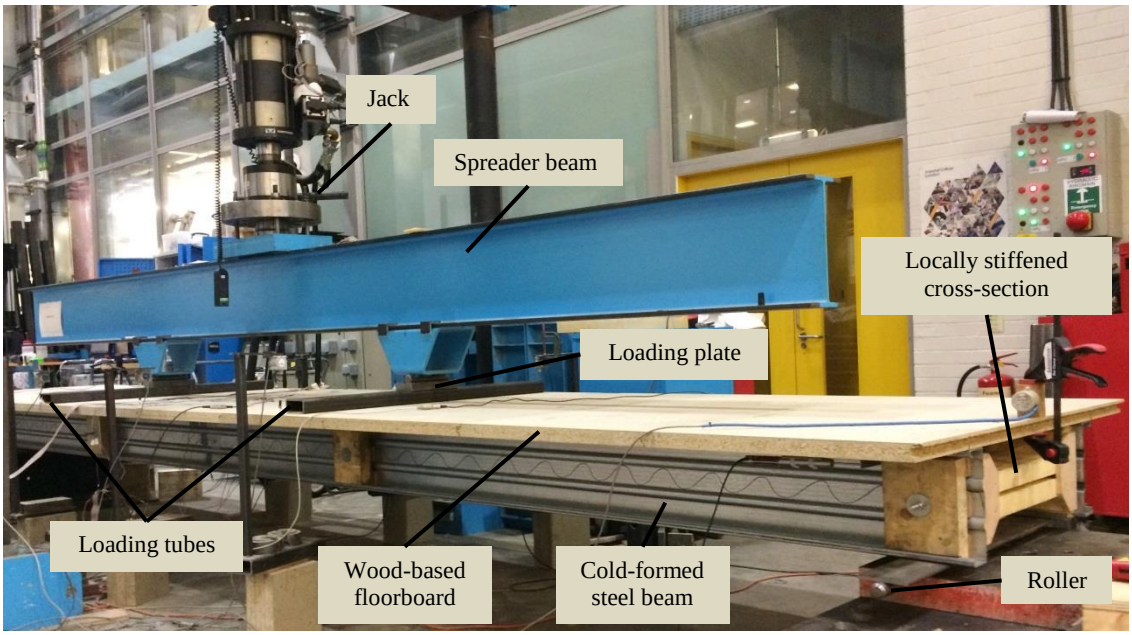


Fig. 12. Experimental layout of composite beam tests

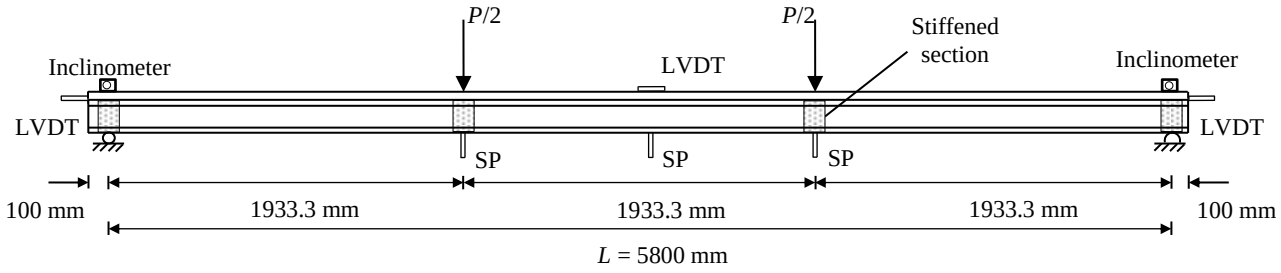


Fig. 13. Employed instrumentation for composite beam tests

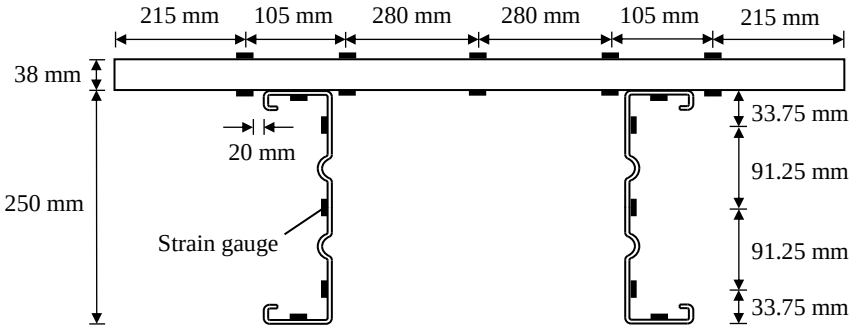


Fig. 14. Positions of strain gauges at the midspan cross-section

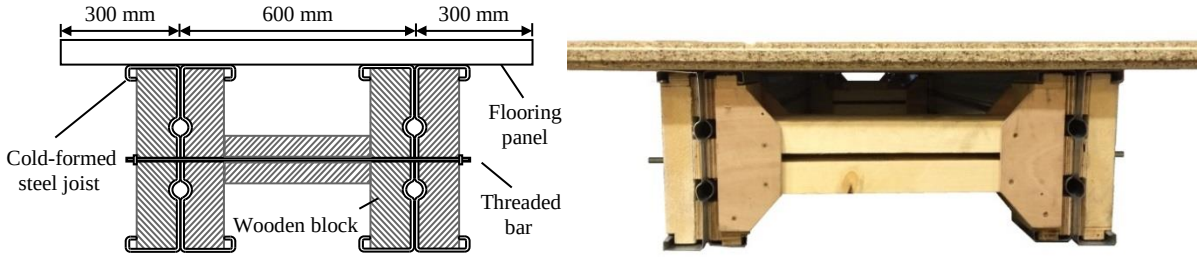


Fig. 15. (a) Schematic illustration and (b) photograph of stiffened cross-section at positions of supports and point loads

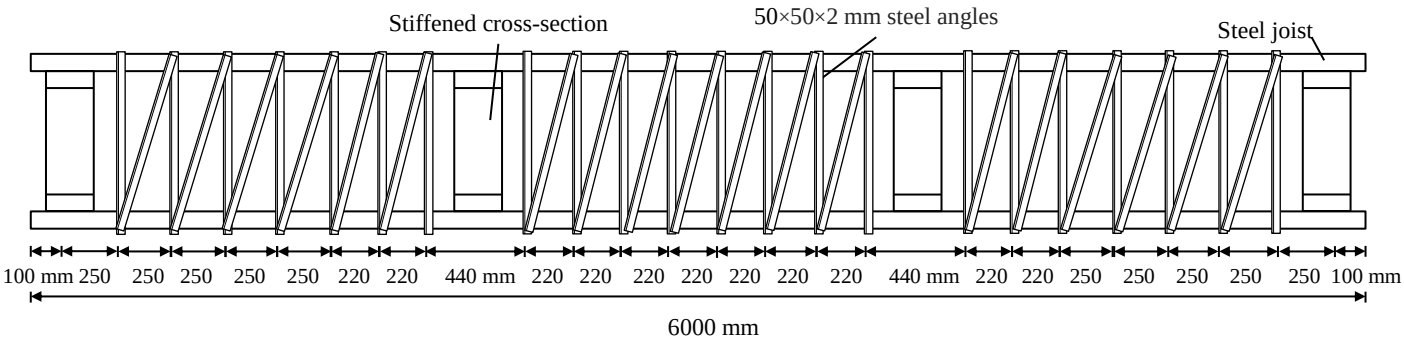
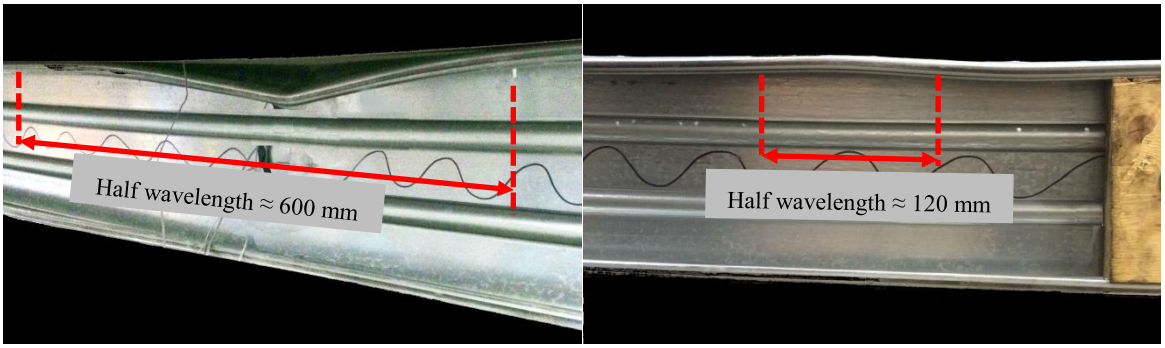


Fig. 16. Plan view of specimen B30-1 (bare steel test)



Fig. 17. Distortional buckling between fixings in the constant moment area (Specimen B30-2)



(a) Specimen B30-2 (b) Specimen B30-6

Fig. 18. Reducing half-wavelength of distortional buckles with reducing screw spacing

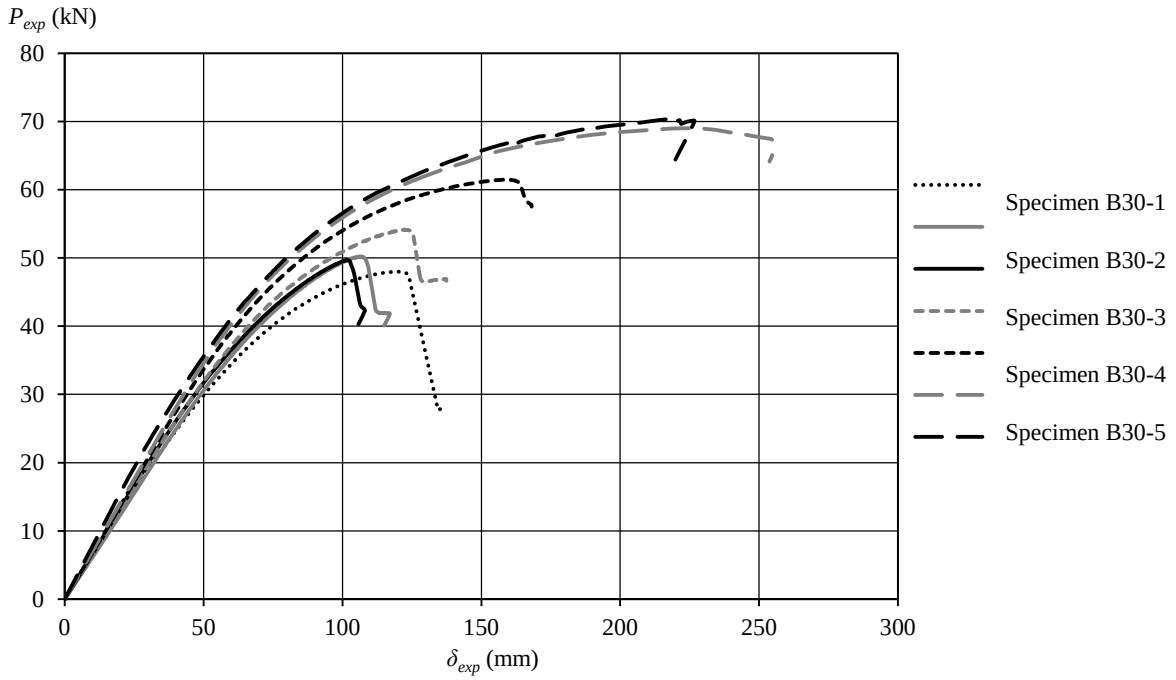


Fig. 19. Load-deflection curves for beam tests with 3 mm thick steel sections

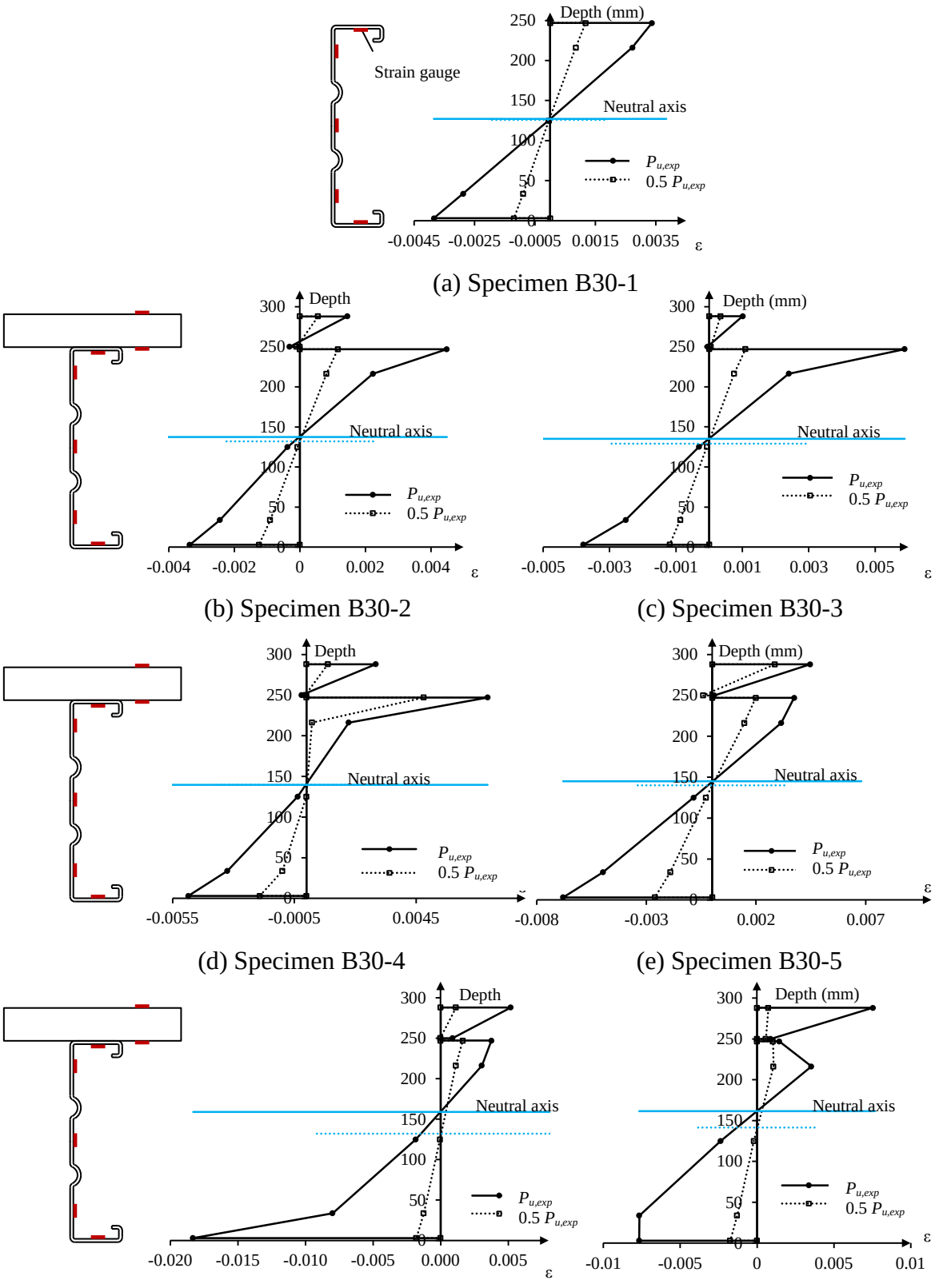


Fig. 20. Strain distributions at midspan sections of all specimens

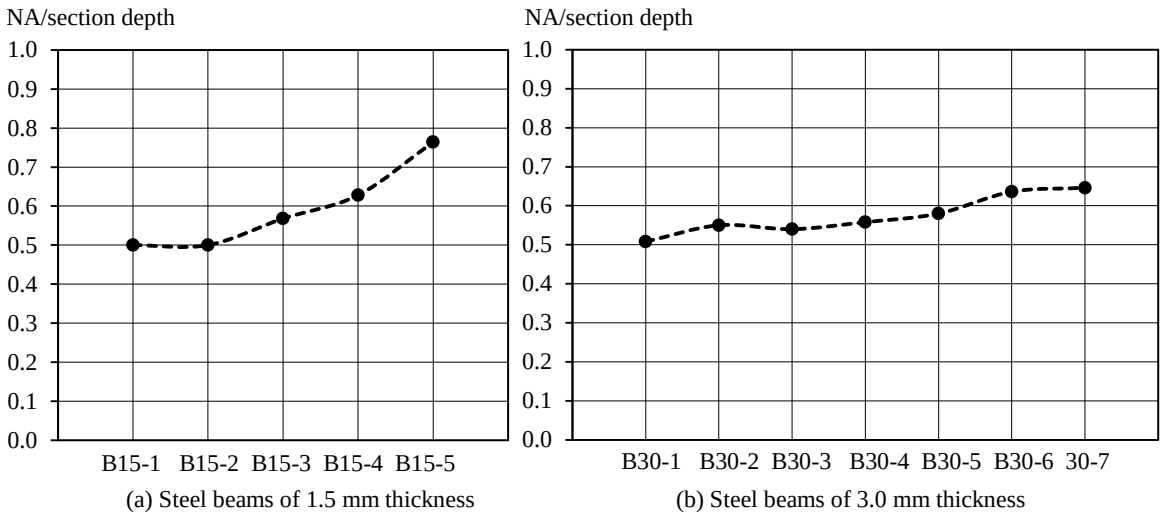


Fig. 21. Position of neutral axis (NA) at ultimate load relative to section depth for all specimens

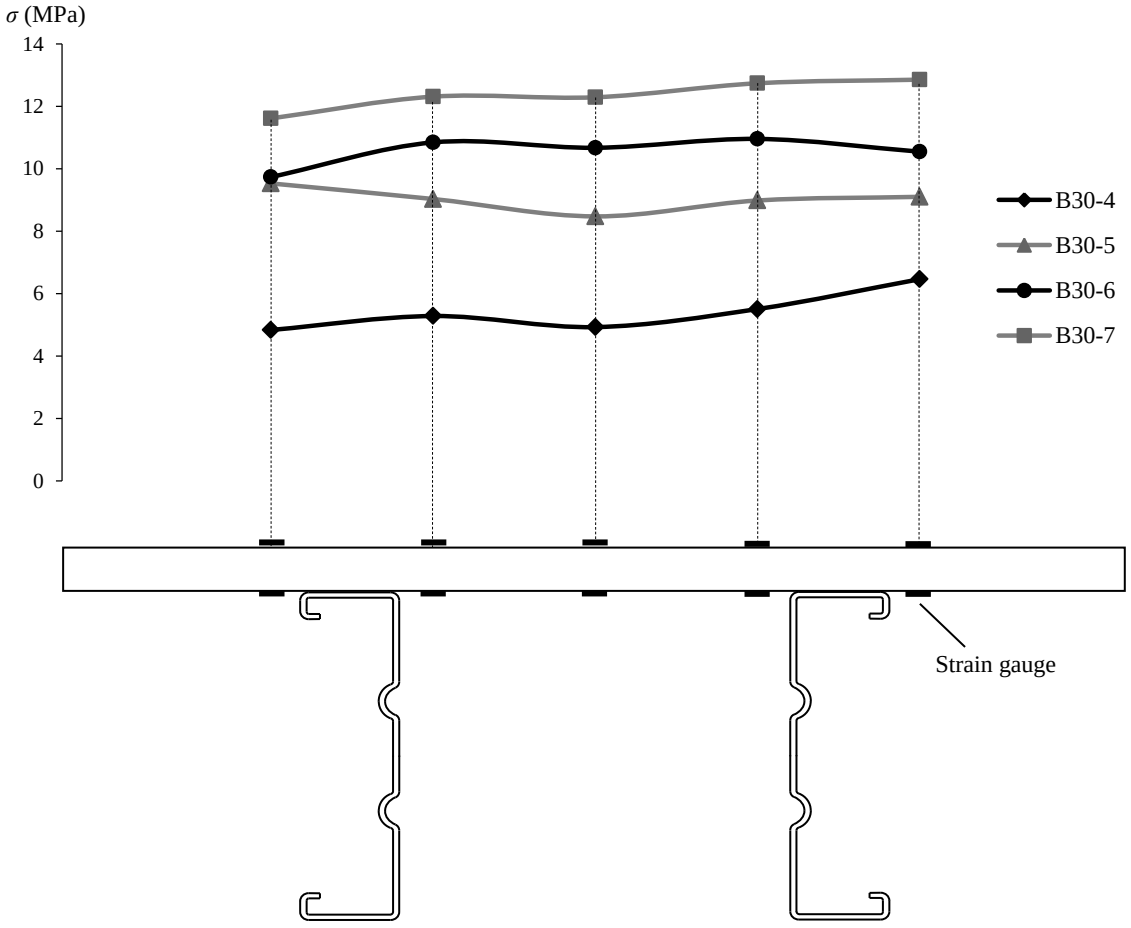
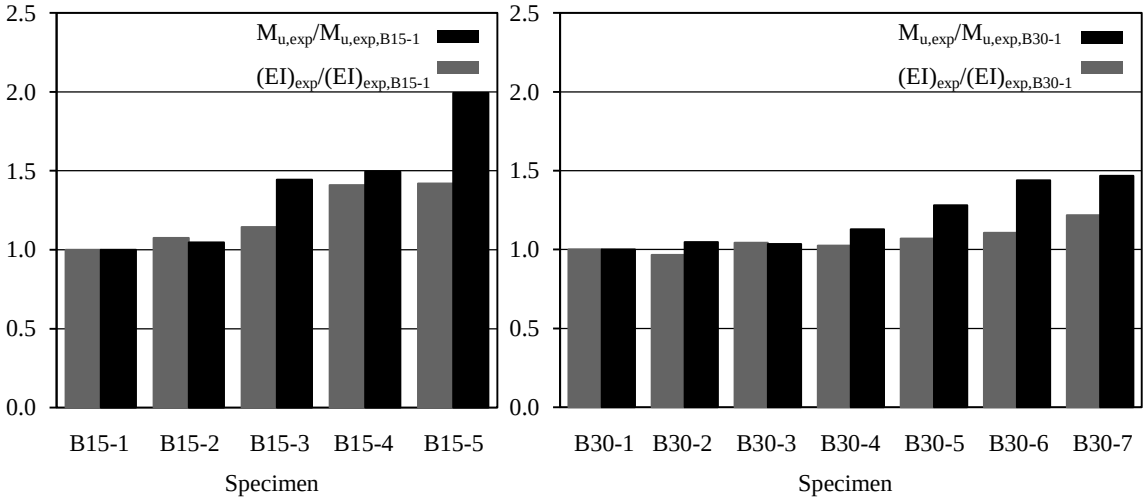


Fig. 22. Stress distributions at the top fiber across the width of the boards



(a) Steel beams of 1.5 mm thickness (b) Steel beams of 3.0 mm thickness

Fig. 23. Enhancements in moment capacity and stiffness of the composite systems relative to the corresponding bare steel system

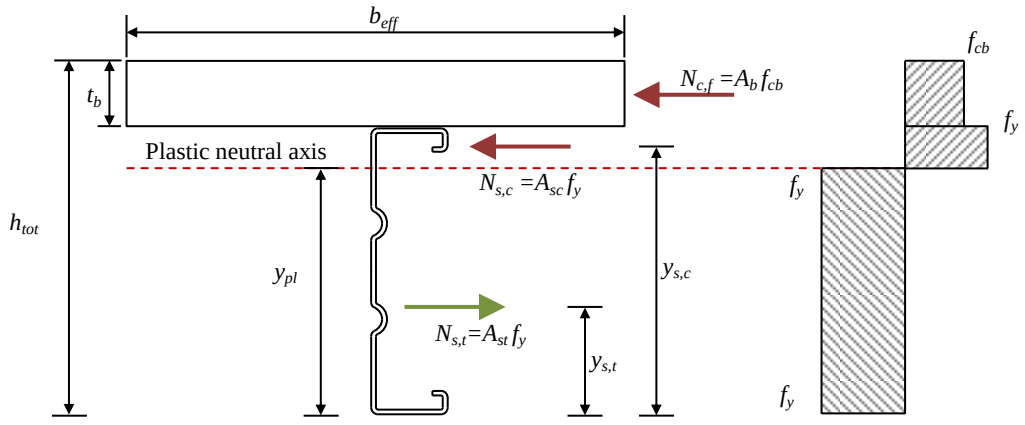


Fig. 24. Plastic stress distribution in a composite section assuming full shear connection

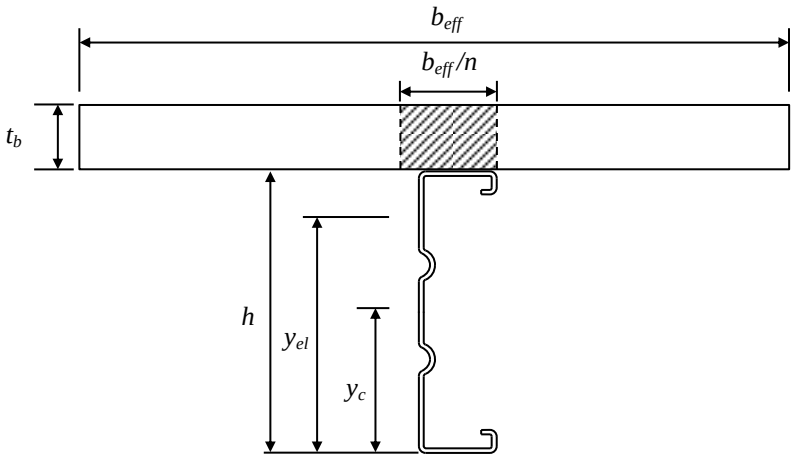
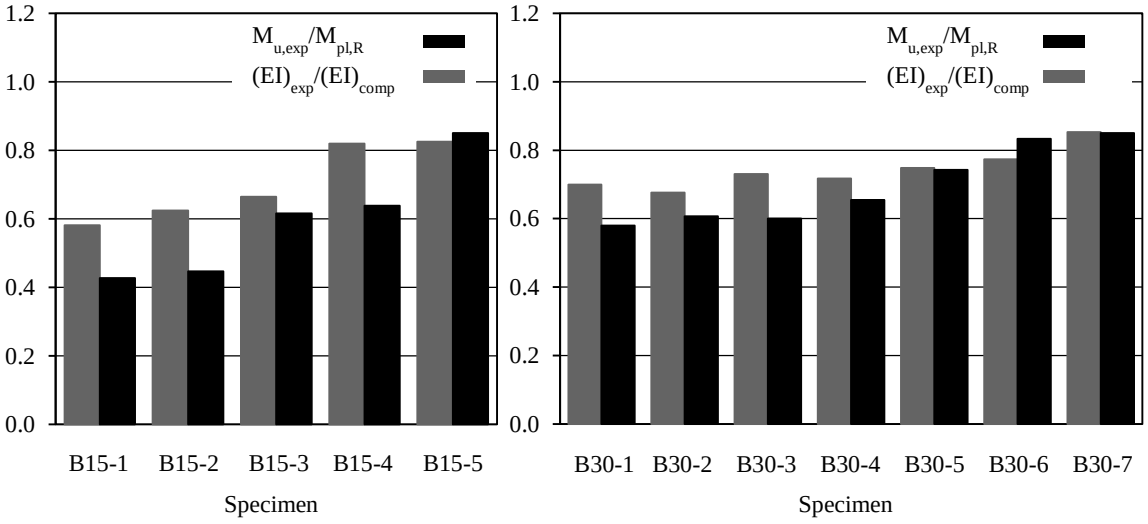
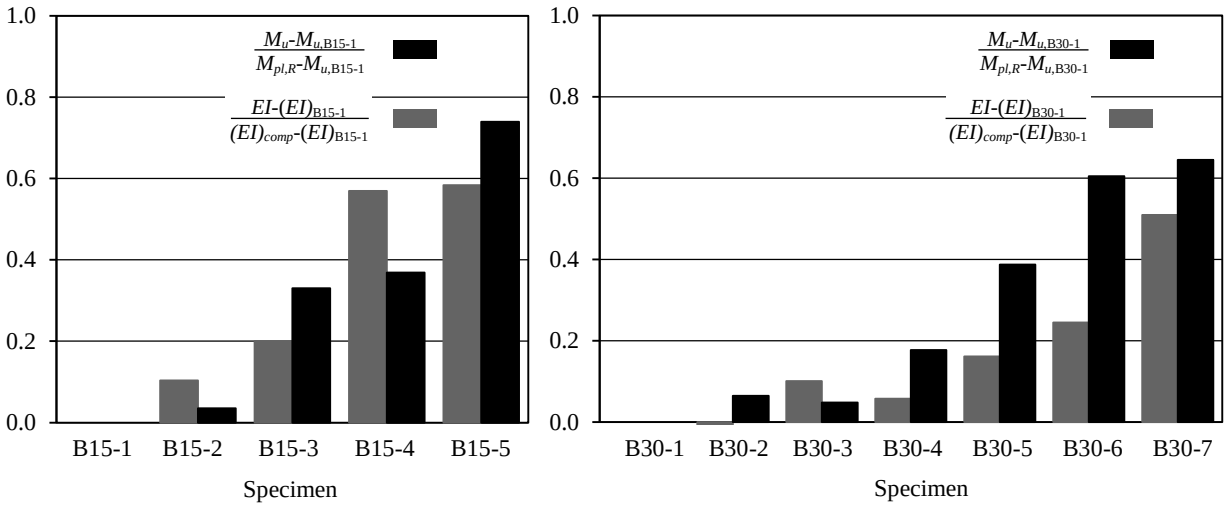


Fig. 25. Transformed section for the determination of the second moment of area of the composite section



(a) Steel beams of 1.5 mm thickness (b) Steel beams of 3.0 mm thickness

Fig. 26. Moment capacity and flexural stiffness of the composite systems relative to the corresponding theoretical fully composite system



(a) Steel beams of 1.5 mm thickness

(b) Steel beams of 3.0 mm thickness

Fig. 27. Test moment capacity and flexural stiffness relative to values for bare steel beam and theoretical fully composite section

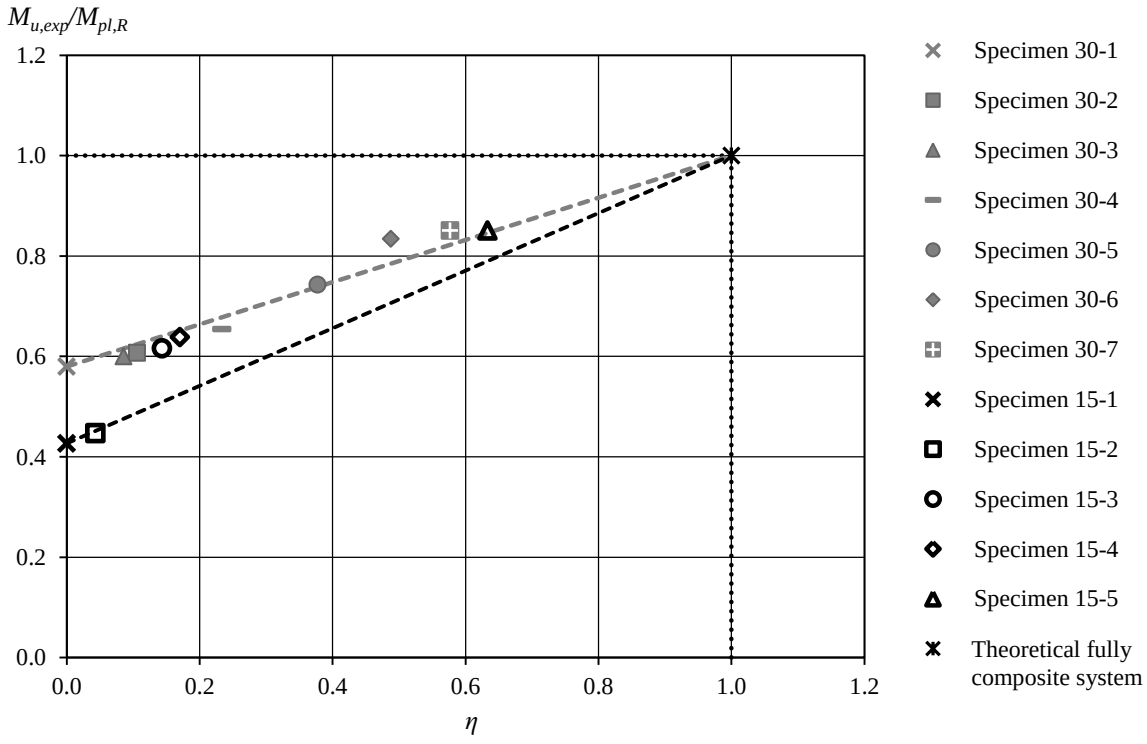
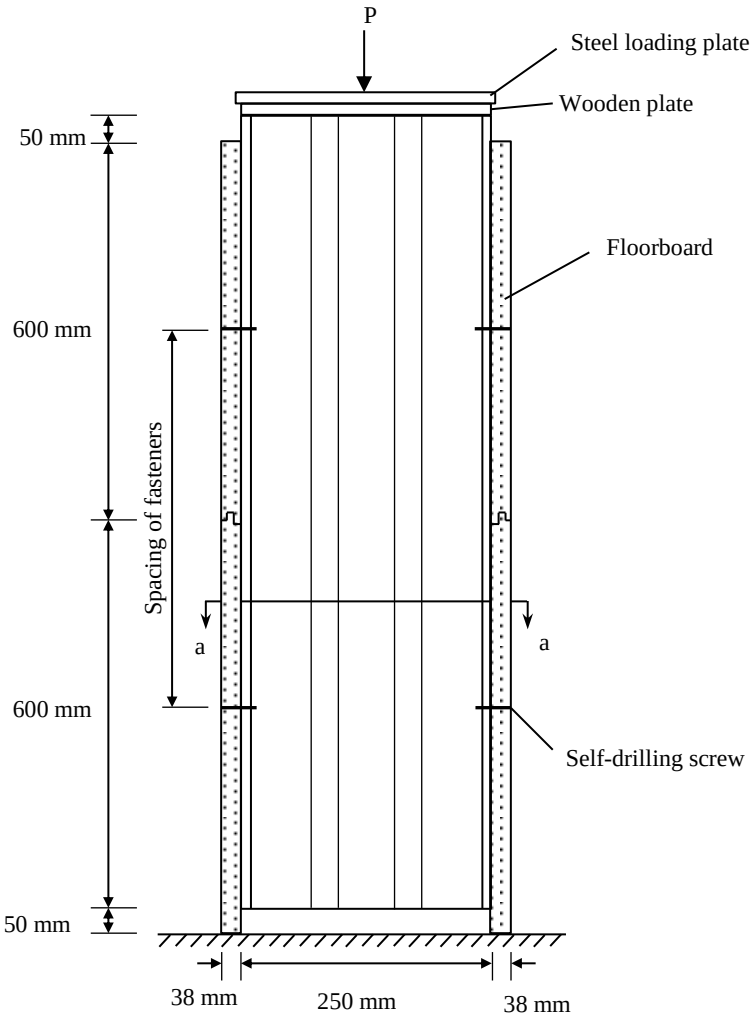
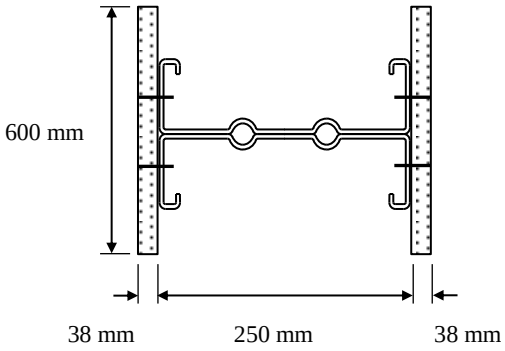


Fig. 28. Attained degree of shear connection for all specimens



(a) Elevation view



(b) Cross-section a-a

Fig. 29. Schematic (a) elevation view and (b) cross-section of push-out specimens

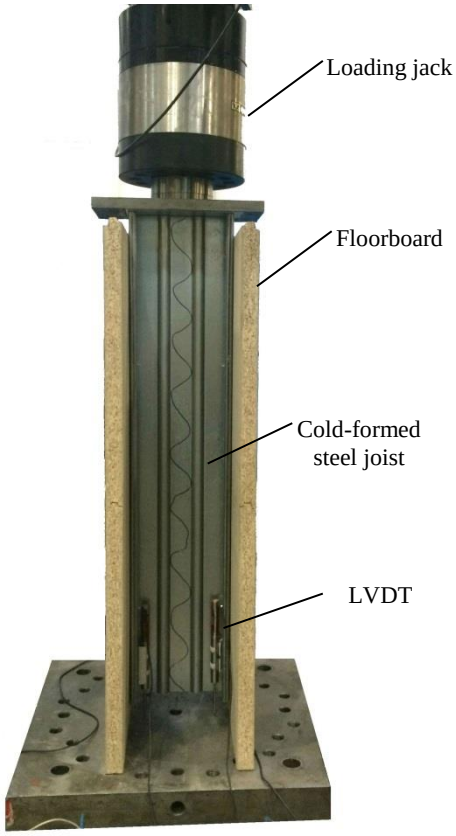


Fig. 30. Experimental setup of push-out tests

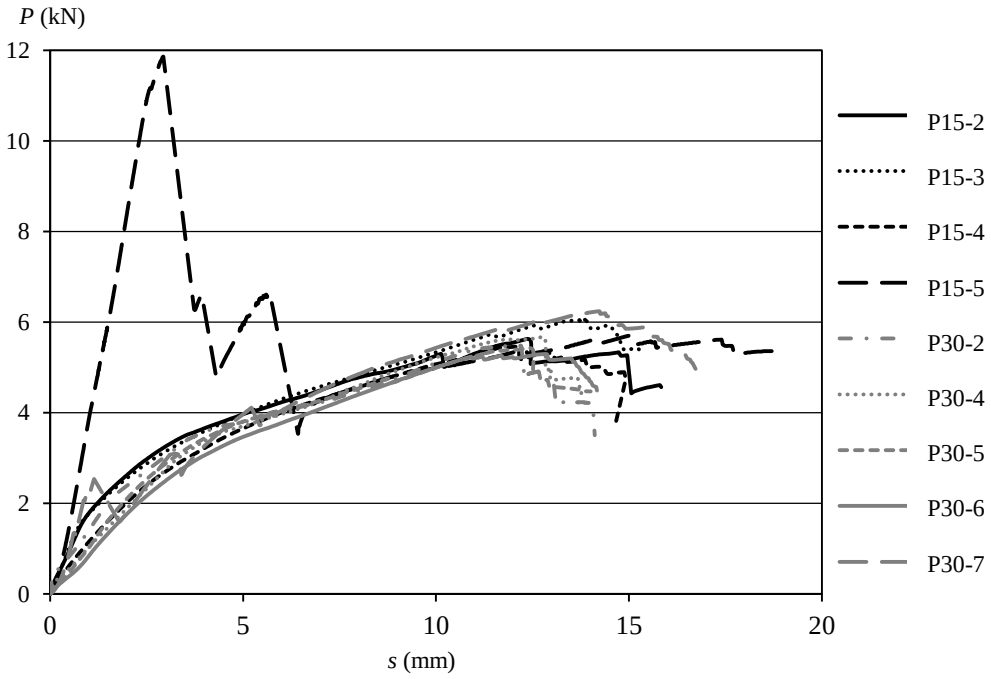
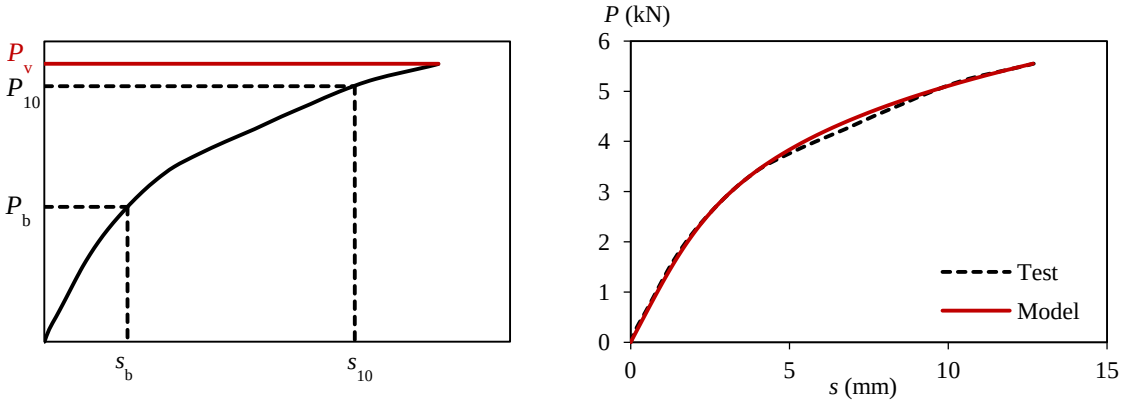


Fig. 31. Load-slip curves from push-out tests



(a) (b)

Fig. 32. Failure modes of push-out specimens: (a) bearing of screw into the board and (b) bending and shear failure of the fasteners



(a) (b)

Fig. 33. Proposed load-slip model: (a) required key points and (b) comparison with the average test curve

Table 1. Material properties of 3 mm thick cold-formed steel sections obtained from tensile coupon tests

Coupon ID	Elastic modulus E (GPa)	Yield strength $\sigma_{0.2}$ (MPa)	Tensile strength σ_u (MPa)	Strain at σ_u ε_u (%)	Elongation at fracture ε_f (%)	n	$n'_{0.2,1.0}$
C30-1 (flat)	209	485	525	10.3	25.8	11.5	1.5
C30-2 (flat)	201	492	512	8.6	35.4	12.1	2.3
C30-3 (flat)	201	476	507	7.3	26.3	13.3	0.7
C30-4 (flat)	201	492	508	7.5	29.7	15.3	1.1
C30-5 (flat)	200	474	514	7.6	31.1	12.6	2.5
C30-6-1 (corner)	207	–	562	0.4	26.9	–	–
C30-6-2 (corner)	194	574	583	0.6	13.1	8.9	3.2
C30-6-3 (corner)	189	560	593	1.0	11.5	6.9	4.1
C30-7-1 (corner)	211	–	640	0.4	11.8	–	–
C30-7-2 (corner)	188	584	605	0.9	11.2	9.7	3.8
C30-7-3 (corner)	193	576	595	0.9	12.4	10.4	3.8

Table 2. Average measured material characteristics of 1.5 mm and 3 mm cold-formed steel sections

Thickness of cold-formed steel coupons t (mm)	Elastic modulus E (GPa)	Flat yield strength $\sigma_{0.2}$ (MPa)	Corner yield strength $\sigma_{0.2}$ (MPa)	Tensile strength σ_u (MPa)	n for flat coupons	$n'_{0.2,1.0}$ for flat coupons	n for corner coupons	$n'_{0.2,1.0}$ for corner coupons
1.51	202	497	573	562	9.5	2.4	13.5	2.5
3.02	200	484	574	559	13.0	1.6	9.0	3.7

Table 3. Average measured material properties of floorboard

Thickness of floorboards t_b (mm)	Elastic modulus in bending E_{mb} (GPa)	Elastic modulus in compression E_{cb} (GPa)	Elastic modulus in tension E_{tb} (GPa)	Bending strength f_{mb} (MPa)	Compressive strength f_{cb} (MPa)	Tensile strength f_{tb} (MPa)
38.06	4.1	2.3	2.1	12.9	12.9	5.8

Table 4. Average dimensions (in mm) of tested cold-formed steel beams

Specimen batch	t	h	b_t	b_b	l_{vt}	l_{vb}	l_{ht}	l_{hb}	a_1	a_2	a_3	b_1	b_2	r_1	r_2
B15	1.51	247.7	63.6	63.3	17.9	17.8	10.0	10.5	67.8	56.3	67.8	27.3	27.8	3.5	12.0
B30	3.02	249.3	64.9	64.9	18.5	18.5	10.9	10.7	61.7	48.8	62.9	35.8	35.9	3.0	12.0

Table 5. Summary of different means of shear connection in tested flooring systems

Specimen	Nominal thickness of steel beam (mm)	Screw spacing (mm)	Wood adhesive at board joints	Epoxy resin at the beam-board interface
B15-1	1.5	n/a	n/a	n/a
B15-2	1.5	600	N	N
B15-3	1.5	150	N	N
B15-4	1.5	150	Y	N
B15-5	1.5	100	Y	Y
B30-1	3.0	n/a	n/a	n/a
B30-2	3.0	600	N	N
B30-3	3.0	600	Y	N
B30-4	3.0	300	N	N
B30-5	3.0	150	N	N
B30-6	3.0	75	N	N
B30-7	3.0	75	Y	Y

Table 6. Key results of 4-point bending tests

Specimen	$M_{u,exp}$ (kNm)	$(EI)_{exp}$ (Nm^2)	$\delta_{u,exp}$ (mm)	$s_{u,exp}$ (mm)	N_c (kN)
B15-1	19.11	1.11×10^6	78.9	–	–
B15-2	20.02	1.19×10^6	72.7	2.4	12.7
B15-3	27.60	1.27×10^6	97.7	1.5	42.1
B15-4	28.58	1.57×10^6	112.6	3.0	50.1
B15-5	38.09	1.58×10^6	179.5	0.0	186.1
B30-1	46.39	2.20×10^6	120.0	–	–
B30-2	48.56	2.13×10^6	106.3	3.4	31.1
B30-3	48.02	2.30×10^6	101.8	4.0	25.2
B30-4	52.35	2.26×10^6	122.2	3.1	68.7
B30-5	59.41	2.36×10^6	159.2	2.3	111.1
B30-6	66.71	2.44×10^6	225.6	1.7	143.4
B30-7	68.06	2.69×10^6	219.1	0.7	169.7

Table 7. Summary of different means of shear connection in push-out tests

Specimen	Thickness of steel beam (mm)	Screw spacing (mm)	Wood adhesive at board joints	Epoxy resin at the beam-board interface
P15-2	1.5	600	N	N
P15-3	1.5	150	N	N
P15-4	1.5	150	Y	N
P15-5	1.5	100	Y	Y
P30-2	3.0	600	N	N
P30-4	3.0	300	N	N
P30-5	3.0	150	N	N
P30-6	3.0	75	N	N
P30-7	3.0	75	Y	Y

Table 8. Summary of results obtained from push-out tests

Specimen No.	P_u (kN)	s_u (mm)
P15-2	5.59	12.45
P15-3	6.05	13.89
P15-4	5.44	12.13
P15-5	–	–
P30-2	5.48	12.18
P30-4	5.64	12.82
P30-5	5.39	12.51
P30-6	5.29	12.87
P30-7	–	–
AVERAGE	5.55	12.69

Table 9. Key measured points for the proposed load-slip model of the fastener

K_o (kN/mm)	P_b (kN)	s_b (mm)	s_{10} (mm)	P_{10} (kN)	P_v (kN)
1.2	2.7	2.7	10.0	5.1	5.6